

# Imitating, Fast and Slow: Robust learning from demonstrations via decision-time planning

Carl Qi,<sup>1</sup> Pieter Abbeel,<sup>2</sup> Aditya Grover<sup>3</sup>

<sup>1</sup> Carnegie Mellon University

<sup>2</sup> University of California, Berkeley

<sup>2</sup> Facebook AI Research

*Abstract*—The goal of imitation learning is to mimic expert behavior from demonstrations, without access to an explicit reward signal. A popular class of approach infers the (unknown) reward function via inverse reinforcement learning (IRL) followed by maximizing this reward function via reinforcement learning (RL). The policies learned via these approaches are however very brittle in practice and deteriorate quickly even with small test-time perturbations due to compounding errors. We propose *Imitation with Planning at Test-time* (IMPLANT), a meta-algorithm for imitation learning that utilizes decision-time planning to correct for compounding errors of any base imitation policy. In contrast to existing approaches, we retain both the imitation policy and the rewards model at decision-time, thereby benefiting from the learning signal of the two components. Empirically, we demonstrate that IMPLANT significantly outperforms benchmark imitation learning approaches on standard control environments and excels at zero-shot generalization when subject to challenging perturbations in test-time dynamics.

*Keywords*—Deep Learning, Imitation Learning, Inverse Reinforcement Learning, Zero-shot Generalization

## I. INTRODUCTION

The objective of imitation learning is to optimize agent policies directly from demonstrations of expert behavior. Such a learning paradigm sidesteps reward engineering, which is a key bottleneck for applying reinforcement learning (RL) in many real-world domains from robotics to autonomous driving. With only a finite dataset of expert demonstrations, however, a key challenge is that the learned policies can quickly deviate from intended expert behavior and lead to compounding errors at test-time [27]. Moreover, it has been observed that imitation policies can be brittle and drastically deteriorate in performance with even small perturbations to the dynamics during execution [9, 13].

A predominant class of approaches to imitation learning is based on inverse reinforcement learning (IRL) and involve successive application of two steps: (a) an IRL step where the agent infers a proxy for the (unknown) reward function for the expert, followed by (b) an RL step where the agent maximizes the inferred reward function via a policy optimization algorithm. For example, many popular IRL approaches consider an adversarial learning framework [15], where the reward function is inferred by a discriminator that distinguishes expert demonstrations from rollouts of an imitation policy [IRL step] and the imitation agent maximizes the inferred reward function to best match the expert policy [RL step] [19, 14]. In this sense, reward inference is only an intermediary step

towards learning the expert policy and is discarded post-training of the imitation agent.

We introduce *Imitation with Planning at Test-time* (IMPLANT), a new meta-algorithm for imitation learning that incorporates decision-time planning into an IRL algorithm. During training, we can use any standard IRL approach to estimate a reward function and a stochastic imitation policy, along with an additional value function. The value function can be learned explicitly or is often a byproduct of standard RL algorithms that involve policy evaluation, such as actor-critic methods [21, 28]. At decision-time, we use the learned imitation policy in conjunction with a closed-loop planner. For any given state, the imitation policy proposes a set of candidate actions and the planner estimates the returns for each of actions by performing fixed-horizon rollouts. The rollout returns are estimated using the learned reward and value functions. Finally, the agent picks the action with the highest return and the process is repeated at each of the subsequent timesteps.

The use of decision-time planning can slow the reaction time of the agent, but can offer significant performance gains. Conceptually, IMPLANT aims to counteract the imperfections due to policy optimization in the RL step by using the proxy reward function (along with a value function) estimated in the IRL step for decision-time planning. We demonstrate strong empirical improvements using this approach over benchmark imitation learning algorithms in a variety of settings derived from the MuJoCo-based benchmarks in OpenAI Gym [43, 4]. In the default evaluation setup where train and test environments match, we observe that IMPLANT improves by 15.7% on average over the closest baseline.

We also consider zero-shot transfer setups where the learned agent is deployed in test dynamics that differ from train dynamics and are inaccessible to the agent during both training and decision-time planning. In particular, we consider the following setups: (a) “causal confusion” where the agent observes nuisance variables in the state representation [13], (b) motor noise which adds noise in the executed action [9], and (c) transition noise which adds noise to the sampled next state. In all setups, we observe that IMPLANT consistently and robustly transfers to test environments with improvements of 52.1% on average over the closest baseline.

## II. BACKGROUND AND SETUP

We consider the framework of Markov Decision Processes (MDP) [31]. An MDP is denoted by a tuple  $\mathcal{M} =$

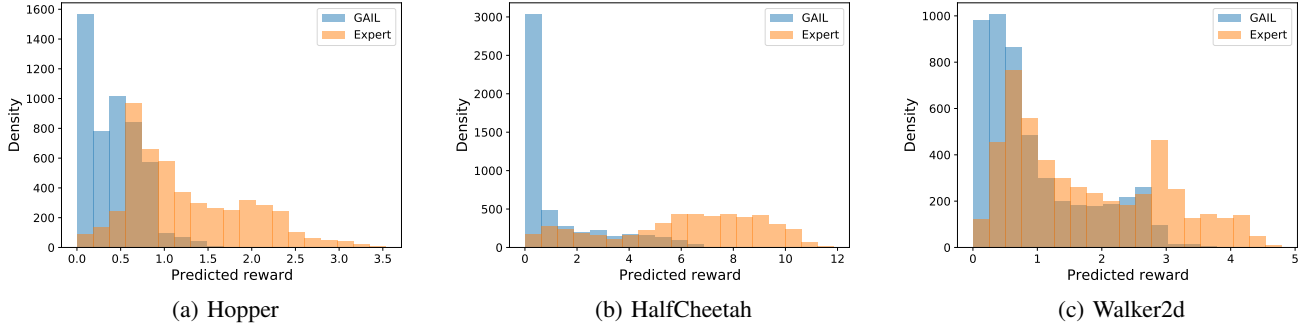


Fig. 1: Distribution of predicted rewards for trained GAIL policies vs. experts.

$(\mathcal{S}, \mathcal{A}, \mathcal{T}, p_0, r, \gamma)$ , where  $\mathcal{S}$  is the state space,  $\mathcal{A}$  is the action space,  $\mathcal{T} : \mathcal{S} \times \mathcal{A} \times \mathcal{S} \rightarrow \mathbb{R}_{\geq 0}$  are the stochastic transition dynamics,  $p_0 : \mathcal{S} \rightarrow \mathbb{R}_{\geq 0}$  is the initial state distribution,  $r : \mathcal{S} \times \mathcal{A} \rightarrow \mathbb{R}$  is the reward function, and  $\gamma \in [0, 1)$  is the discount factor. We assume an infinite horizon setting. At any given state  $s \in \mathcal{S}$ , an agent makes decisions via a stochastic policy  $\pi : \mathcal{S} \times \mathcal{A} \rightarrow \mathbb{R}_{\geq 0}$ . We denote a trajectory to be a sequence of state-action pairs  $\tau = (s_0, a_0, s_1, a_1, \dots)$ . Any policy  $\pi$ , along with MDP parameters, induces a distribution over trajectories, which can be expressed as  $p_\pi(\tau) = p(s_0) \prod_{t=0}^{\infty} \pi(a_t | s_t) \mathcal{T}(s_{t+1} | s_t, a_t)$ . The return of a trajectory is the discounted sum of rewards  $R(\tau) = \sum_{t=0}^{\infty} \gamma^t r(s_t, a_t)$ .

In reinforcement learning (RL), the goal is to learn a parameterized policy  $\pi_\theta$  that maximizes the expected returns w.r.t. the trajectory distribution. Maximizing such an objective requires interaction with the underlying MDP for simulating trajectories and querying rewards. However, in many high-stakes scenarios, the reward function is not directly accessible and hard to manually design.

In imitation learning, we sidestep the availability of the reward function. Instead, we have access to a finite set of  $D$  trajectories  $\tau_E$  (a.k.a. demonstrations) that are sampled from an expert policy  $\pi_E$ . Every trajectory  $\tau \in \tau_E$  consists of a finite-length sequence of state and action pairs  $\tau = (s_0, a_0, s_1, a_1, \dots)$ , where  $s_0 \sim p_0(s)$ ,  $a_t \sim \pi_E(\cdot | s_t)$ , and  $s_{t+1} \sim \mathcal{T}(\cdot | s_t, a_t)$ . Our goal is to learn a parameterized policy  $\pi_\theta$  which best approximates the expert policy given access to  $\tau_E$ . Next, we discuss the two major families of techniques for imitation learning.

### A. Behavioral Cloning

Behavioral cloning (BC) casts imitation learning as a supervised learning problem over state-action pairs provided in the expert demonstrations [30]. In particular, we learn the policy by solving a regression problem with states  $s_t$  and actions  $a_t$  as the features and target labels respectively. Formally, we minimize the following objective:

$$\ell_{BC}(\theta) := \sum_{(s_t, a_t) \in \tau_E} \|a_t - \pi_\theta(s_t)\|_2^2. \quad (1)$$

In practice, BC agents suffer from *distribution shift* in high dimensions, where small deviations in the learned policy

accumulate during deployment and lead to a significantly different trajectory distribution relative to the expert [37, 38].

### B. Inverse Reinforcement Learning

An alternative indirect approach to imitation learning is based on inverse reinforcement learning (IRL). Here, the goal is to infer a reward function for the expert and subsequently maximize the inferred reward to obtain a policy. For brevity, we focus on adversarial imitation learning approaches to IRL [15]. These approaches represent the state-of-the-art in imitation learning and are also relevant baselines for our empirical evaluations.

Generative Adversarial Imitation Learning (GAIL) is an IRL algorithm that formulates imitation learning as an ‘‘occupancy measure matching’’ objective w.r.t. a suitable probabilistic divergence [19]. GAIL consists of two parameterized networks: (a) a policy network  $\pi_\theta$  (generator) which is used to rollout agent trajectories (assuming access to transition dynamics), and (b) a discriminator  $D_\phi$  which distinguishes between ‘‘real’’ expert demonstrations and ‘‘fake’’ agent trajectories. Given expert trajectories  $\tau_E$  and agent trajectories  $\tau_\theta$ , the discriminator minimizes the cross-entropy loss:

$$\ell_{IRL}(\phi) := -\mathbb{E}_{\tau_E} [\log D_\phi(\tau_E)] - \mathbb{E}_{\tau_\theta} [\log(1 - D_\phi(\tau_\theta))]. \quad (2)$$

We then feed the discriminator output  $-\log(1 - D_\phi(s, a))$  as the inferred reward function to the generator policy. The policy parameters  $\theta$  can be updated via any standard policy optimization algorithm, *e.g.*, Ho and Ermon [19] use the TRPO algorithm [39]. By simulating agent rollouts, GAIL seeks to match the full trajectory state-action distribution of the imitation agent with the expert as opposed to BC which greedily matches the conditional distribution of individual actions given the states. In practice, GAIL and its variants [24, 14] outperform BC but might need excessive interactions with the training environment for sampling rollouts. Crucially, both BC and IRL approaches tend to fail catastrophically in the presence of small perturbations and nuisances at test-time [13].

## III. THE IMPLANT FRAMEWORK

In the previous section, we showed that imitation learning algorithms based on IRL consider reward inference as an

---

**Algorithm 1: Imitation with Planning at Test-time (IMPLANT)**


---

**Input:** available dynamics  $\hat{\mathcal{T}}$ , expert demonstrations  $\tau_E$ , rollout budget  $B$ , rollout policy  $\pi$ , horizon  $H$ , test start state  $s_0$

**Note:** For brevity, we omit relevant MDP parameters in the list of arguments.

```

1 Function Train( $\tau_E$ ):
2   Learn a policy  $\pi_\theta$  and a reward function  $r_\phi$  with
   any existing IRL algorithm given access to
   demonstrations  $\tau_E$ , e.g., GAIL
3   Estimate a value function  $V_\psi$  for  $\pi_\theta$ 
4   return  $\pi_\theta, r_\phi, V_\psi$ ;

5 Function Plan( $s, \pi_\theta, V_\psi, r_\phi, \pi, H, B, \hat{\mathcal{T}}$ ):
6   Set  $s = s_0$ 
7   while agent is alive do
8     /* Agent planning */
9     Sample  $B$  trajectories  $\{\tau^{(1)}, \tau^{(2)}, \dots, \tau^{(B)}\}$  of
     max length  $H$  starting from  $s$  using dynamics
      $\hat{\mathcal{T}}$ ; sample the first action  $a_0^{(i)} \sim \pi_\theta$ , and
     sample subsequent actions from  $\pi$  as  $a_{>0}^{(i)} \sim \pi$ ,
     for  $i \in \{1, 2, \dots, B\}$ 
10    Estimate trajectory returns  $\hat{R}_{\phi, \psi}(\tau^{(i)})$  using  $V_\psi$ 
     and  $r_\phi$  (see Eq. 4)
11    Pick best action index  $i^* = \arg \max_i \hat{R}_{\phi, \psi}(\tau^{(i)})$ 
     and execute the best action  $a_0^{(i^*)}$ 
12    /* Environment feedback */
13    Observe true reward  $r(s, a_0^{(i^*)})$  and true next
     state  $s \sim \mathcal{T}(\cdot | s, a_0^{(i^*)})$ 
14  end

```

---

auxiliary task. Once the agents have been trained, the reward function is discarded and the learned policy is deployed. Indeed, if the RL step post reward inference (e.g., generator updates in GAIL) were optimal, then the reward function provides no additional information about the expert relative to the imitation policy. However, this is far from reality, as current RL algorithms can fail to return optimal solutions due to either representational or optimization issues. For example, there might be a mismatch in the architecture of the policy network and the expert policy, and/or difficulties in optimizing non-convex objective functions.

In fact, the latter challenge gets exacerbated in adversarial learning scenarios due to a non-stationary reward. For reference, we consider the policies and discriminator-based rewards learned via GAIL. Ideally, we would expect the distribution of inferred discriminator-based rewards for the (state, action) distribution induced by the expert to match the imitation policy (generator) post-training. We show the empirical distribution of rewards for three MuJoCo environments in Figure 1. As we can see, there are noticeable differences in the empirical distribution of rewards for the learned agents and the expert, suggesting the challenges in fully exploiting the reward signal inferred through the discriminator simply via policy optimization in the

RL step.

Building off these observations, we propose *Imitation with Planning at Test-time* (IMPLANT), an imitation learning algorithm that employs the learned reward function for decision-time planning. The pseudocode for IMPLANT is shown in Algorithm 1. We can dissect IMPLANT into two sequential phases: a training phase and a planning phase.

a) *Training phase*:: We can invoke any imitation learning algorithm, e.g., GAIL, that optimizes for a stochastic imitation policy  $\pi_\theta$  to maximize some inferred reward function  $r_\phi$ . Given the challenges due to non-identifiability of the true reward function in imitation learning [26], the inferred reward function is typically only a proxy signal for learning e.g., discriminator outputs in adversarial methods [19, 14], unsupervised perceptual rewards for self-supervised imitation learning [40], etc.

We also train a parameterized value function  $V_\psi$  at this stage. Value function estimation is often a subroutine for many RL algorithms including those used to update the policy within the IRL setup, such as actor-critic methods [21]. For such algorithms, learning a value function does not incur any additional computation.

b) *Planning phase*:: At decision-time, we use the imitation policy along with the learned value and reward functions for closed-loop planning. We build our planner based on model-predictive control (MPC) [7]. At any given state  $s_t$  and time  $t \geq 0$ , we are interested in choosing action sequences for trajectories which maximizes the following objective:

$$a_t, a_{t+1}, \dots, = \arg \max_{a_t, a_{t+1}, \dots} R(\tau) = \sum_{t'=t}^{\infty} \gamma^{t'-t} r(s_{t'}, a_{t'}) \quad (3)$$

where  $s_0 \sim p_0$  and  $s_{t+1} \sim \mathcal{T}(\cdot | s_t, a_t)$  for all  $t \geq 0$ .

This objective has also been applied for model-based RL with a learned dynamics model and black-box access to the rewards function [25, 10]. Unlike the RL setting, however, we do not know the reward function for imitation learning. We will assume access to some approximation of the true dynamics such as a simulator [19] or a model estimated from expert demonstrations and/or training interactions [3]. As we shall demonstrate in our experiments, IMPLANT is robust even when the true dynamics  $\mathcal{T}$  perturb from the dynamics available for planning  $\hat{\mathcal{T}}$ . Given  $\hat{\mathcal{T}}$ , we can do rollouts as before in regular model-based RL but need to rely on learned estimates for the reward function. In particular, we use the learned reward function  $r_\phi$  up to a fixed horizon  $H$  and a terminal value function  $V_\psi$  thereafter to estimate the trajectory return as:

$$R(\tau) \approx \sum_{t'=t}^{t+H-1} \gamma^{t'-t} r_\phi(s_{t'}, a_{t'}) + \gamma^H V_\psi(s_H) := \hat{R}_{\phi, \psi}(\tau). \quad (4)$$

Substituting Eq. 4 in Eq. 3, we obtain a surrogate objective for optimization. To optimize this surrogate, we propose a variant of the random shooting optimizer [36] that works as follows. At the current state  $s_t$ , we first sample a set of  $B$  candidate actions independently from the imitation policy. For each candidate action, we estimate a score based on their expected returns by performing rollout(s) of fixed-length  $H$ .

TABLE I: Average return of imitation learning algorithms on MuJoCo benchmarks.

	Hopper	HalfCheetah	Walker2d
Expert	3570	9892	4585
BC	127 $\pm$ 85	-359 $\pm$ 247	153 $\pm$ 162
BC-Dropout	169 $\pm$ 105	-99 $\pm$ 229	344 $\pm$ 72
GAIL	3506 $\pm$ 337	4059 $\pm$ 728	3847 $\pm$ 635
GAIL-Reward Only	319 $\pm$ 123	-284 $\pm$ 77	2 $\pm$ 5
IMPLANT (ours)	<b>3633</b> $\pm$ 50	<b>5240</b> $\pm$ 924	<b>4403</b> $\pm$ 242

The rollout policy  $\pi$  from which we sample all subsequent actions could be random (potentially high variance) or the imitation policy  $\pi_\theta$  (potentially high bias) or a mixture. In our experiments, we obtained consistently better performance with using  $\pi_\theta$  as the rollout policy  $\pi$  and taking the mean of  $\pi$  instead of sampling. For each trajectory, we estimate its return via Eq. 4 and finally, pick the action with the largest return.

Consistent with the closed-loop nature of MPC, we repeat the above procedure at the next state  $s_t$ . Doing so helps correct for errors in estimation and optimization in the previous time step, albeit at the expense of additional computation. The algorithm has two critical parameters that induce similar computational trade-offs. First, we need to specify a budget  $B$  for the total number of rollouts. The higher the budget, larger is our search space for the best action. Second, we need to specify a planning horizon  $H$ . For larger lengths, we need extra computation to interact with the dynamics of the environment and rely more on the learned reward function than the value function for estimating returns in Eq. 4. However, since the rollouts are independent, we can mitigate additional computational costs by parallelizing them. While this parallelization is indeed bottlenecked by the last finished rollout, in all of our experiments, we perform rollouts of fixed length and the optimal horizon is relatively small ( $10 \sim 50$ ). Thus, the gains due to parallelization are significant.

#### IV. EXPERIMENTS

Our experiments aim to evaluate IMPLANT in two kinds of settings. First, we evaluate its performance in the default “no-transfer” setting, where the agent is trained and tested in the same environment. Second, we emphasize the robustness of IMPLANT by evaluating its zero-shot generalization performance in environments where the test dynamics are a perturbed version of the training dynamics. We consider three such perturbations: causal confusion [13], motor noise [9], and transition noise. We will describe each of these setups subsequently alongside the results. For all transfer settings, we only assume access to the training simulator and use it as  $\hat{\mathcal{T}}$  for planning. At test-time, no additional interactions is allowed, nor do we have access to the test dynamics  $\mathcal{T}_{test}$ .

*a) Setup.:* We evaluate our approach on MuJoCo environments in OpenAI Gym [4]: Hopper, HalfCheetah, and Walker2d. We obtain the expert data by training a SAC agent [18]. We replicate the experimental setup of Ho and Ermon [19] by fixing a limited number of expert trajectories used for training, as well as sub-sampling expert trajectories every 20 time steps. All results are averaged over 5 runs of each algorithm with different seeds. We provide further details in Appendix A.

*b) Baselines.:* As we observed in Algorithm 1, IMPLANT can employ any IRL algorithm under the hood. For our experiments, we consider GAIL [19] as the IRL algorithm of choice both as input for IMPLANT and consequently, as the closest baseline of interest. GAIL is amongst the current state-of-the-art methods for imitation learning; see Section II-B for a detailed description. For every environment, we report results for IMPLANT using a single set of hyperparameters for the rollout budget and planning horizon. We provide further details in Appendix A.

Additionally, we consider a Behavioral Cloning (BC) baseline; see Section II-A for a detailed description. We also tested variants of GAIL and BC with dropout [41] to demonstrate the limited utility of standard regularization techniques in countering the challenges due to low data and test noise. In fact, GAIL with dropout completely failed to learn in the adversarial setting on all environments; for brevity, we exclude it from presentation.

Last, we include a “GAIL-Reward Only” ablation baseline where we discard the imitation policy (generator) of GAIL during execution and instead, only use the inferred reward model (discriminator) in conjunction with a random policy for decision-time planning. This directly contrasts with the GAIL baseline, which by default only uses the generator. On the other hand, IMPLANT uses both the generator and discriminator for imitation via decision-time planning.

##### A. Imitation with Limited Expert Trajectories

With a very low number of expert trajectories, Ho and Ermon [19] showed that GAIL achieves excellent performance in almost all these environments. In the first set of experiments, we test IMPLANT under the same constraints to estimate its raw performance (without any test-time perturbations). The results are shown in Table I. We find that IMPLANT consistently outperforms existing algorithms on all environments. It also achieves near-optimal performance, with the exception of HalfCheetah, where even GAIL performs noticeably worse than the expert. As expected, BC and BC-Dropout perform poorly in this setting. GAIL-Reward Only exhibits the poorest performance suggesting the benefits of explicitly learning a parametric policy.

##### B. Zero-Shot Transfer: Causal Confusion

de Haan et al. [13] observed that imitation learning approaches are susceptible to *causal confusion*, i.e., their performance deteriorates significantly in the presence of nuisance

TABLE II: Average return of imitation learning algorithms in causal confusion: action nuisance.

	Hopper	HalfCheetah	Walker2d
Expert	3570	9892	4585
BC	209 ± 121	-297 ± 308	160 ± 135
BC-Dropout	162 ± 108	-159 ± 300	230 ± 120
GAIL	579 ± 484	1367 ± 660	2052 ± 745
GAIL-Reward Only	515 ± 302	-90 ± 90	114 ± 191
IMPLANT (ours)	<b>1717 ± 1262</b>	<b>3890 ± 1080</b>	<b>3891 ± 585</b>

TABLE III: Average return of imitation learning algorithms in causal confusion: state nuisance.

	Hopper	HalfCheetah	Walker2d
Expert	3570	9892	4585
BC	203 ± 115	-409 ± 233	91 ± 175
BC-Dropout	213 ± 135	-207 ± 229	422 ± 85
GAIL	1733 ± 1402	2492 ± 748	2628 ± 1237
GAIL-Reward Only	362 ± 41	-38 ± 131	125 ± 197
IMPLANT (ours)	<b>3642 ± 85</b>	<b>5465 ± 889</b>	<b>4527 ± 308</b>

confounders in the state representation. To demonstrate this phenomena empirically, de Haan et al. [13] further propose a challenging setup in which the nuisance is created by appending the agent’s observation with its action from the previous time step. A standard imitation agent trained in this setup will learn to *copy* the previous action (since successive actions are highly correlated in expert demonstrations), falling prey to causal confusion. At test-time, the agent’s performance drops drastically if the appended action is replaced by random noise (*i.e.*, the confounding is removed). We refer the reader to de Haan et al. [13] for further details and analysis. We benchmark IMPLANT and other imitation learning algorithms under two causal confusion setups:

- 1) **Action nuisance.** This follows de Haan et al. [13], where the action from the previous step is appended to the observation to create nuisance.
- 2) **State nuisance.** Alternatively, we can corrupt the observation directly by appending a nuisance variable  $s$  to the observation that correlates with high reward in the training environment but is absent at test time. For example, in locomotion environments such as Hopper, when the agent crosses a certain velocity threshold ( $v \geq v_{th}$ ), we set  $s = 1$ . At test time, the nuisance is disabled completely *i.e.*,  $s = 0$ .

The results are shown in Table II and Table III. While all baselines, including GAIL, fail due to the confounding nuisance, IMPLANT is significantly more robust in all environments. Impressively, IMPLANT is able to completely overcome the nuisance and recover the non-confounded policy performance (Table I) in all 3 environments with state nuisance. We can visualize the agent performance qualitatively in Figure 4. Note that we provided the IMPLANT agent access to only the confounded dynamics for decision-time planning. The algorithm is zero-shot, unlike the proposed solutions of Fu et al. [14] and de Haan et al. [13] which require further interactions with the non-confounded test environment for recovery.

### C. Zero-Shot Transfer: Motor and Transition Noise

Next, we consider two kinds of noisy perturbations motivated by real-world applications in sim2real. First, we perturb the intended actions via **motor noise** [9], *e.g.*, due to imperfect hardware, a real robot might execute a noisy version of the action proposed by the agent. We implement this scenario by adding independent Gaussian noise to each dimension of the executed action at test-time, *i.e.*,  $\epsilon_{\text{action}} \stackrel{i.i.d.}{\sim} \mathcal{N}(0, \sigma^2)$  and we vary the noise stddev  $\sigma \in [0.1, 0.2, 0.5, 1.0]$ .

Second, we consider **transition noise** due to an imperfect dynamics model for a simulator that may not be able to account for perturbations due to drag or friction. Hence, we specify the test-time dynamics to be a perturbed noisy version of the training dynamics. Similar to motor noise, we sample the transition noise as  $\epsilon_{\text{transition}} \stackrel{i.i.d.}{\sim} \mathcal{N}(0, \sigma^2)$  with  $\sigma \in [0.001, 0.002, 0.005, 0.01]$ .

For ease of visualization, we show the normalized performance of the different algorithms in Figure 2. See Appendix B for raw absolute results. We also include another competitive baseline “GAIL-Expert-Noise” relevant to this scenario that artificially adds independent noise to the demonstration data for every gradient update during GAIL training. For a very high noise level, any algorithm will naturally deteriorate in performance due to significant shift in training and testing environments. More importantly, for modest noise levels, we find that IMPLANT outperforms the baselines in almost all cases, highlighting its robustness.

### D. Effect of Planning Horizon

Finally, we analyze the effect of planning horizon on IMPLANT performance in the same setup as Section IV-A. Specifically, we vary the planning horizon  $H \in [0, 10, 50, 100]$  for a rollout budget  $B = 10$ . The normalized performance curves are shown in Figure 3. When the planning horizon is 0, we only rely on the terminal value function for estimating returns. Conversely, for large planning horizons (*e.g.*,  $H = 100$ ), the returns are dominated by rewards accumulated at every time step. We observe that picking neither a very large horizon ( $h \geq 100$ ) nor a very small one ( $h = 0$ ) results

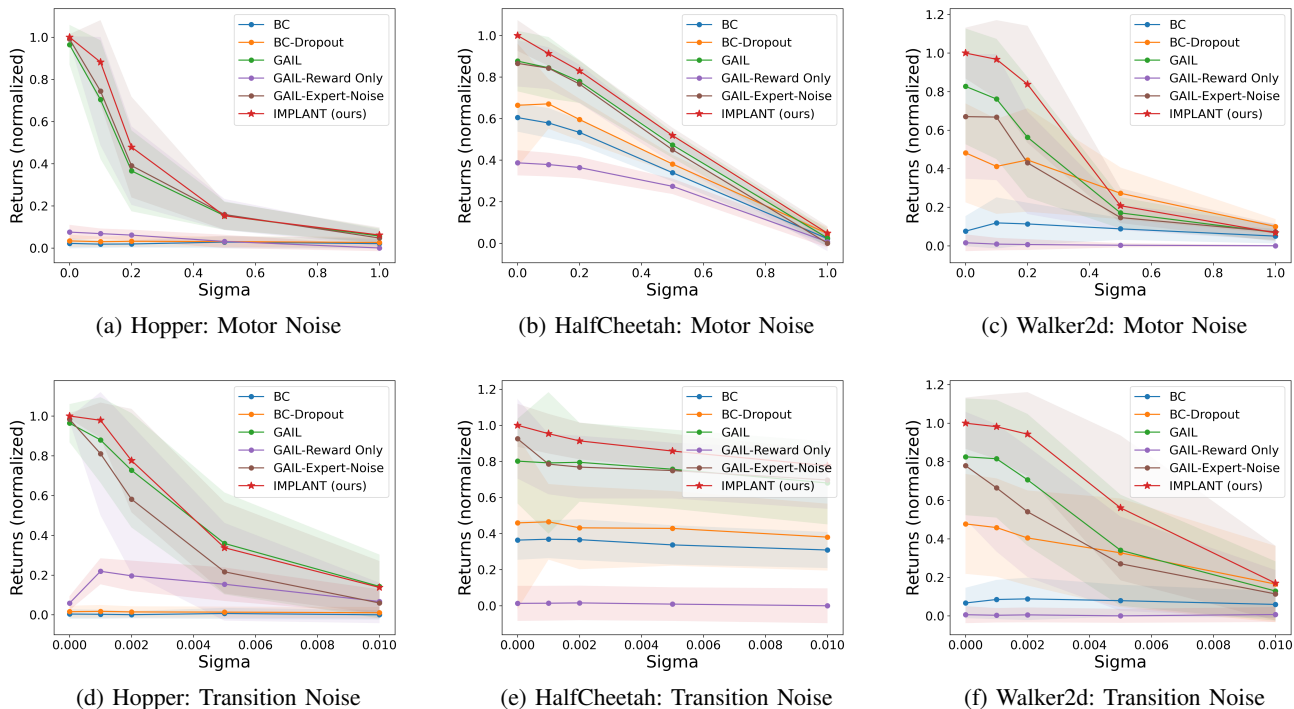


Fig. 2: Avg. return of imitation learning algorithms on motor and transition noise; shaded region shows std. error over 5 runs.

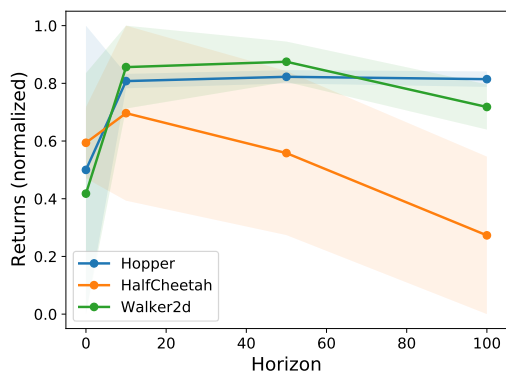


Fig. 3: Effect of planning horizon  $H$  on IMPLANT; returns are normalized; shaded region shows std. error over 5 runs.

in optimal performance, suggesting imperfections in both the learned reward and value functions and the sweet-spot for the planning horizon is typically between the extremes.

## V. DISCUSSION & RELATED WORK

Traditionally, algorithms for imitation learning fall into one of two categories. They are either completely model-free during both training and execution, e.g., behavioral cloning and its variants [30, 38]. Alternatively, they are model-based in the sense that they utilize dynamics and (inferred) rewards models during training, but are model-free during execution, as in inverse reinforcement learning [26, 32, 46]. Our work introduces a novel model-based perspective to imitation learning where the reward and transition models are used *both* during training and execution. Borrowing the terminology from

Sutton and Barto [42], the use of such models during training and execution are also referred to as *background* and *decision-time* planning respectively.

While imitation via background planning has been used for control in complex environments [1, 33, 19, 8], we showed that decision-time planning in IMPLANT can further improve the data efficiency and robustness of the learned policies. There have also been several alternate attempts for characterizing and enhancing the robustness of imitation policies. For example, Fu et al. [14] seek robustness in the sense of recovering the true reward function via adversarial imitation learning and transfer the inferred reward function to external dynamics in the non-zero shot setting. A significant body of work also considers IRL approaches that can capture the uncertainty in the reward function for safe deployment [45, 5, 20, 23, 6]. While these utility-based notions are distinct from ours, they are complementary approaches to robustness that could be combined with IMPLANT in future work. Finally, we note there has been prior work in using imitation learning *for* planning in autonomous driving domain [34, 35, 12]. These approaches learn a dynamics model of future states given the past from the expert demonstrations and leverage this model for planning. Although these methods demonstrate their robustness in out-of-distribution environments, they require the access of a controller to output the low-level actions, which we do not assume to be available.

Given the synergies between generative modeling and imitation learning as exemplified in GAIL [19], improvements in the former often translate into improved imitation, e.g., the use of autoencoder embeddings to improve diversity [44], better loss functions and architectures for stable GAN/GAIL

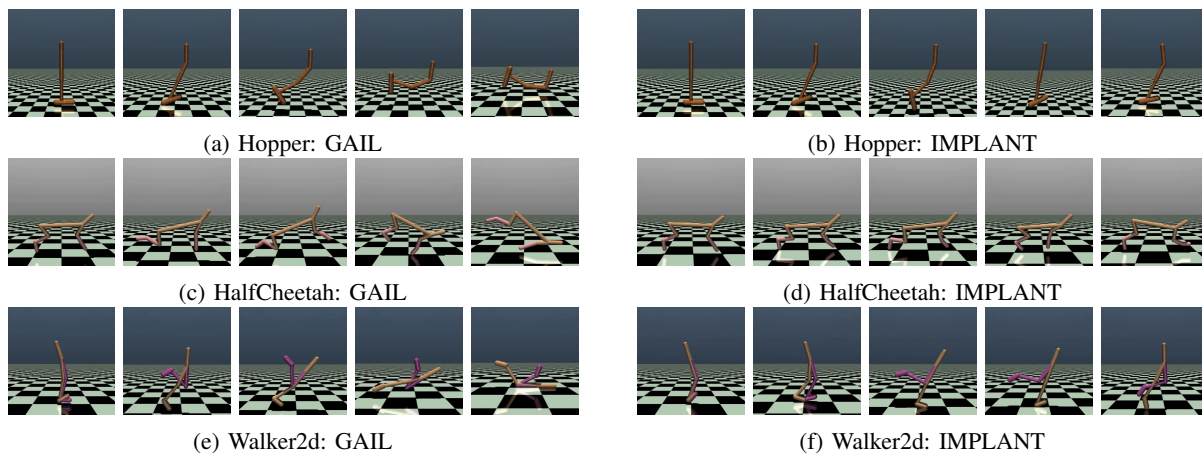


Fig. 4: Trajectory visualization for causal confusion: state nuisance at test-time. While all agents start from the same state (see first frame), only IMPLANT can effectively move forward. All agents are trained in the confounded setting and tested in the non-confounded setting.

training [29, 22, 24], etc. These modifications are conceptually complementary to the key contribution of IMPLANT to incorporate decision-time planning and are likely to further boost our performance. In fact, decision-time planning in IMPLANT can be viewed as filtering of trajectories sampled from the policy network. This is similar to recent work in using importance weighting for improving sample quality of a generative model [16, 2, 17]. However, our solution is tailored towards sequential decision making, provides flexibility in model rollouts, and deterministically picks the best outcome in line with model predictive control, unlike importance weighting filters.

## VI. CONCLUSION

We presented *Imitation with Planning at Test-time* (IMPLANT), a new meta-algorithm for imitation learning that uses decision-time planning to mitigate compounding errors of any base IRL-based imitation learning algorithm. Unlike existing approaches, IMPLANT is truly model-based in the sense of utilizing the inferred rewards and dynamics model both during training and execution. While decision-time planning is in general *slower* than simply executing a feed-forward policy, we argue that it can be much more accurate and robust than model-free execution of imitation policies. We demonstrated that IMPLANT matches or outperforms existing benchmark imitation learning algorithms with very few expert trajectories. Finally, we empirically demonstrated the robustness of IMPLANT via its impressive performance at zero-shot generalization in several challenging perturbation settings involving causal confusion [13] and noisy perturbations to the environment dynamics and policy execution.

## REFERENCES

- [1] P. Abbeel and A. Y. Ng. Apprenticeship learning via inverse reinforcement learning. In *Proceedings of the twenty-first international conference on Machine learning*, page 1, 2004.
- [2] S. Azadi, C. Olsson, T. Darrell, I. Goodfellow, and A. Odena. Discriminator rejection sampling. *arXiv preprint arXiv:1810.06758*, 2018.
- [3] N. Baram, O. Anschel, and S. Mannor. Model-based adversarial imitation learning. *arXiv preprint arXiv:1612.02179*, 2016.
- [4] G. Brockman, V. Cheung, L. Pettersson, J. Schneider, J. Schulman, J. Tang, and W. Zaremba. Openai gym. *arXiv preprint arXiv:1606.01540*, 2016.
- [5] D. S. Brown, Y. Cui, and S. Niekum. Risk-aware active inverse reinforcement learning. In *Conference on Robot Learning*, pages 362–372, 2018.
- [6] D. S. Brown, S. Niekum, and M. Petrik. Bayesian robust optimization for imitation learning. *arXiv preprint arXiv:2007.12315*, 2020.
- [7] E. F. Camacho and C. B. Alba. *Model predictive control*. Springer Science & Business Media, 2013.
- [8] S. Choudhury, M. Bhardwaj, S. Arora, A. Kapoor, G. Ranade, S. Scherer, and D. Dey. Data-driven planning via imitation learning. *The International Journal of Robotics Research*, 37(13-14):1632–1672, 2018.
- [9] P. Christiano, Z. Shah, I. Mordatch, J. Schneider, T. Blackwell, J. Tobin, P. Abbeel, and W. Zaremba. Transfer from simulation to real world through learning deep inverse dynamics model. *arXiv preprint arXiv:1610.03518*, 2016.
- [10] K. Chua, R. Calandra, R. McAllister, and S. Levine. Deep reinforcement learning in a handful of trials using probabilistic dynamics models. In *Advances in Neural Information Processing Systems*, pages 4754–4765, 2018.
- [11] R. Dadashi, L. Hussenot, M. Geist, and O. Pietquin. Primal wasserstein imitation learning, 2020.
- [12] N. Dashora, D. Shin, D. Shah, H. Leopold, D. Fan, A. Agha, N. Rhinehart, and S. Levine. Hybrid imitative

- planning with geometric and predictive costs in offroad environments. In *Deep RL Workshop NeurIPS 2021*, 2021. URL <https://openreview.net/forum?id=b5CAA57Mozr>.
- [13] P. de Haan, D. Jayaraman, and S. Levine. Causal confusion in imitation learning. In *Advances in Neural Information Processing Systems*, pages 11698–11709, 2019.
- [14] J. Fu, K. Luo, and S. Levine. Learning robust rewards with adversarial inverse reinforcement learning. *arXiv preprint arXiv:1710.11248*, 2017.
- [15] I. Goodfellow, J. Pouget-Abadie, M. Mirza, B. Xu, D. Warde-Farley, S. Ozair, A. Courville, and Y. Bengio. Generative adversarial nets. In *Advances in neural information processing systems*, pages 2672–2680, 2014.
- [16] A. Grover and S. Ermon. Boosted generative models. *arXiv preprint arXiv:1702.08484*, 2017.
- [17] A. Grover, J. Song, A. Kapoor, K. Tran, A. Agarwal, E. J. Horvitz, and S. Ermon. Bias correction of learned generative models using likelihood-free importance weighting. In *Advances in Neural Information Processing Systems*, pages 11058–11070, 2019.
- [18] T. Haarnoja, A. Zhou, P. Abbeel, and S. Levine. Soft actor-critic: Off-policy maximum entropy deep reinforcement learning with a stochastic actor, 2018.
- [19] J. Ho and S. Ermon. Generative adversarial imitation learning. In *Advances in neural information processing systems*, pages 4565–4573, 2016.
- [20] J. Huang, F. Wu, D. Precup, and Y. Cai. Learning safe policies with expert guidance. In *Advances in Neural Information Processing Systems*, pages 9105–9114, 2018.
- [21] V. R. Konda and J. N. Tsitsiklis. Actor-critic algorithms. In *Advances in neural information processing systems*, pages 1008–1014, 2000.
- [22] A. Kuefler, J. Morton, T. Wheeler, and M. Kochenderfer. Imitating driver behavior with generative adversarial networks. In *2017 IEEE Intelligent Vehicles Symposium (IV)*, pages 204–211. IEEE, 2017.
- [23] J. Lacotte, M. Ghavamzadeh, Y. Chow, and M. Pavone. Risk-sensitive generative adversarial imitation learning. In *The 22nd International Conference on Artificial Intelligence and Statistics*, pages 2154–2163. PMLR, 2019.
- [24] Y. Li, J. Song, and S. Ermon. Infogail: Interpretable imitation learning from visual demonstrations. In *Advances in Neural Information Processing Systems*, pages 3812–3822, 2017.
- [25] A. Nagabandi, G. Kahn, R. S. Fearing, and S. Levine. Neural network dynamics for model-based deep reinforcement learning with model-free fine-tuning. In *2018 IEEE International Conference on Robotics and Automation (ICRA)*, pages 7559–7566. IEEE, 2018.
- [26] A. Y. Ng, S. J. Russell, et al. Algorithms for inverse reinforcement learning. In *Icml*, volume 1, page 2, 2000.
- [27] T. Osa, J. Pajarinen, G. Neumann, J. A. Bagnell, P. Abbeel, and J. Peters. An algorithmic perspective on imitation learning. *arXiv preprint arXiv:1811.06711*, 2018.
- [28] J. Peters and S. Schaal. Natural actor-critic. *Neurocomputing*, 71(7-9):1180–1190, 2008.
- [29] D. Pfau and O. Vinyals. Connecting generative adversarial networks and actor-critic methods. *arXiv preprint arXiv:1610.01945*, 2016.
- [30] D. A. Pomerleau. Efficient training of artificial neural networks for autonomous navigation. *Neural computation*, 3(1):88–97, 1991.
- [31] M. L. Puterman. Markov decision processes. *Handbooks in operations research and management science*, 2:331–434, 1990.
- [32] N. D. Ratliff, J. A. Bagnell, and M. A. Zinkevich. Maximum margin planning. In *Proceedings of the 23rd international conference on Machine learning*, pages 729–736, 2006.
- [33] N. D. Ratliff, D. Silver, and J. A. Bagnell. Learning to search: Functional gradient techniques for imitation learning. *Autonomous Robots*, 27(1):25–53, 2009.
- [34] N. Rhinehart, R. McAllister, and S. Levine. Deep imitative models for flexible inference, planning, and control. In *International Conference on Learning Representations*, 2020. URL <https://openreview.net/forum?id=Sk14mRNYDr>.
- [35] N. Rhinehart, J. He, C. Packer, M. A. Wright, R. McAllister, J. E. Gonzalez, and S. Levine. Contingencies from observations: Tractable contingency planning with learned behavior models. *arXiv preprint arXiv:2104.10558*, 2021.
- [36] A. G. Richards. *Robust constrained model predictive control*. PhD thesis, Massachusetts Institute of Technology, 2005.
- [37] S. Ross and D. Bagnell. Efficient reductions for imitation learning. In *Proceedings of the thirteenth international conference on artificial intelligence and statistics*, pages 661–668, 2010.
- [38] S. Ross, G. Gordon, and D. Bagnell. A reduction of imitation learning and structured prediction to no-regret online learning. In *Proceedings of the fourteenth international conference on artificial intelligence and statistics*, pages 627–635, 2011.
- [39] J. Schulman, S. Levine, P. Abbeel, M. Jordan, and P. Moritz. Trust region policy optimization. In *International conference on machine learning*, pages 1889–1897, 2015.
- [40] P. Sermanet, K. Xu, and S. Levine. Unsupervised perceptual rewards for imitation learning. *arXiv preprint arXiv:1612.06699*, 2016.
- [41] N. Srivastava, G. Hinton, A. Krizhevsky, I. Sutskever, and R. Salakhutdinov. Dropout: A simple way to prevent neural networks from overfitting. *Journal of Machine Learning Research*, 15(56):1929–1958, 2014.
- [42] R. S. Sutton and A. G. Barto. *Reinforcement learning: An introduction*. MIT press, 2018.
- [43] E. Todorov, T. Erez, and Y. Tassa. Mujoco: A physics engine for model-based control. In *2012 IEEE/RSJ International Conference on Intelligent Robots and Systems*, pages 5026–5033. IEEE, 2012.
- [44] Z. Wang, J. S. Merel, S. E. Reed, N. de Freitas, G. Wayne, and N. Heess. Robust imitation of diverse behaviors. In *Advances in Neural Information Processing Systems*, pages 5320–5329, 2017.
- [45] J. Zheng, S. Liu, and L. M. Ni. Robust bayesian inverse

reinforcement learning with sparse behavior noise. In *Proceedings of the Twenty-Eighth AAAI Conference on Artificial Intelligence*, pages 2198–2205, 2014.

- [46] B. D. Ziebart, A. L. Maas, J. A. Bagnell, and A. K. Dey. Maximum entropy inverse reinforcement learning. In *Aaai*, volume 8, pages 1433–1438. Chicago, IL, USA, 2008.

## APPENDIX A ADDITIONAL EXPERIMENTAL DETAILS

TABLE IV: Environment characteristics.

Environment	Observation space	Action space
Hopper	Box(11, )	Box(3, )
HalfCheetah	Box(17, )	Box(6, )
Walker2d	Box(17, )	Box(6, )

### A. Environments and Expert Data

As mentioned above, we consider 3 continuous tasks from OpenAI Gym [4] simulated with MuJoCo [43]: Hopper, HalfCheetah, and Walker2d. We acquire expert data by training a SAC [18] agent with ground truth reward and then recording its rollouts. Table IV lists more detailed information about each environment, and Table V contains information about the expert demonstrations we use for training all of the agents.

### B. Hyperparameters and Network Architectures

We use a 2-layer MLP with *tanh* activations and 100 hidden units for all of our policy networks. For BC, we use a learning rate of  $10^{-4}$  across all environments. We use a dropout rate of 0.2 for our BC-Dropout agent. The hyperparameters of GAIL are listed in Table VI.

For our IMPLANT agent, we directly utilize the value function, reward function, and policy from a trained GAIL agent. Further, we set  $B = 20$  and  $H = 50$  for Hopper,  $B = 2$  and  $H = 10$  for HalfCheetah, and  $B = 20$  and  $H = 50$  for Walker2d for MPC planning.

TABLE V: Expert dataset characteristics.

Environment	# trajectories	# state-action pairs	expert performance
Hopper	4	200	3570
HalfCheetah	4	200	9892
Walker2d	4	200	4585

## APPENDIX B ADDITIONAL RESULTS

### A. Raw Performance of Motor Noise and Transition Noise

The complete results for Section IV-C can be found in Table VII, VIII, IX.

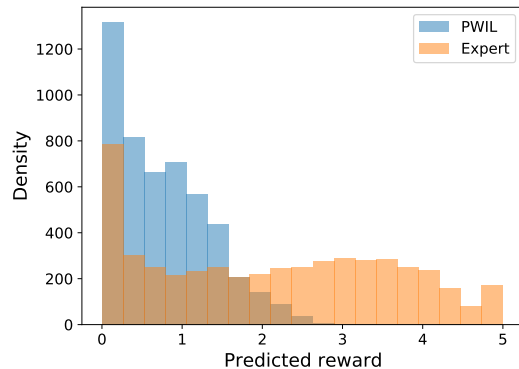


Fig. 5: Distribution of predicted rewards for trained PWIL policy vs. expert in Hopper.

### B. Robustifying other IRL algorithms

In principle, IMPLANT is a meta-algorithm and hence can be used as a wrapper for improving the robustness of any IRL-based imitation learning algorithm. To demonstrate the general-purposeness, we perform planning with a very recent state-of-the-art imitation learning algorithm, Primal Wasserstein Imitation Learning (PWIL) [11] in Hopper environment. Unlike GAIL, PWIL is a non-adversarial algorithm and exhibits impressive sample efficiency in terms of interactions with the environment.

Figure 5 shows a mismatch in the distributions of rewards for policy rollouts and expert, as predicted by the reward function for PWIL, suggesting the benefits of planning using the same reward function at test-time. Tables X and XI show the improvements in performance via IMPLANT for the setups with motor noise and transition noise perturbations respectively.

TABLE VI: Hyperparameters used for GAIL training.

Parameters	Hopper	HalfCheetah	Walker2d
Discriminator network	100-100 MLP	100-100 MLP	100-100 MLP
Discriminator entropy coeff.	0.01	0.01	0.01
Batch size	1024	50000	50000
Max kl	0.01	0.01	0.01
CG steps/damping	10, 0.01	10, 0.1	10, 0.1
Entropy coeff.	0.0	0.0	0.0
Value fn. steps/step size	3, 3e-4	5,3e-4	5,3e-4
Generator steps	3	3	3
Discriminator steps	1	1	1
$\lambda$	0.98	0.97	0.97
$\gamma$	0.99	0.995	0.995

TABLE VII: Raw results of Figure 2 in Hopper environment

(a) Hopper with motor noise

Sigma	0.0	0.1	0.2	0.5	1.0
BC	127 $\pm$ 85	114 $\pm$ 64	117 $\pm$ 61	179 $\pm$ 105	123 $\pm$ 82
BC-Dropout	169 $\pm$ 105	156 $\pm$ 85	163 $\pm$ 95	158 $\pm$ 89	142 $\pm$ 94
GAIL	3506 $\pm$ 337	2572 $\pm$ 1008	1360 $\pm$ 687	598 $\pm$ 243	252 $\pm$ 128
GAIL-Reward Only	319 $\pm$ 123	293 $\pm$ 87	268 $\pm$ 92	160 $\pm$ 113	49 $\pm$ 54
GAIL-Expert-Noise	3602 $\pm$ 46	2716 $\pm$ 921	1449 $\pm$ 667	<b>618</b> $\pm$ 264	218 $\pm$ 136
IMPLANT (ours)	<b>3633</b> $\pm$ 50	<b>3209</b> $\pm$ 714	<b>1764</b> $\pm$ 856	596 $\pm$ 234	<b>269</b> $\pm$ 130

(b) Hopper with transition noise

Sigma	0.0	0.001	0.002	0.005	0.01
BC	127 $\pm$ 85	123 $\pm$ 81	116 $\pm$ 65	137 $\pm$ 98	114 $\pm$ 84
BC-Dropout	169 $\pm$ 105	175 $\pm$ 113	165 $\pm$ 99	161 $\pm$ 98	151 $\pm$ 101
GAIL	3506 $\pm$ 337	3209 $\pm$ 756	2672 $\pm$ 1012	<b>1377</b> $\pm$ 901	<b>616</b> $\pm$ 563
GAIL-Reward Only	319 $\pm$ 123	884 $\pm$ 230	804 $\pm$ 269	665 $\pm$ 296	349 $\pm$ 215
GAIL-Expert-Noise	3576 $\pm$ 36	2966 $\pm$ 1089	2160 $\pm$ 1311	875 $\pm$ 865	323 $\pm$ 357
IMPLANT (ours)	<b>3633</b> $\pm$ 50	<b>3557</b> $\pm$ 313	<b>2844</b> $\pm$ 915	1301 $\pm$ 810	598 $\pm$ 467

TABLE VIII: Raw results of Figure 2 in HalfCheetah environment

(a) HalfCheetah with motor noise

Sigma	0.0	0.1	0.2	0.5	1.0
BC	-359 $\pm$ 247	-375 $\pm$ 238	-355 $\pm$ 241	-409 $\pm$ 175	-873 $\pm$ 102
BC-Dropout	-99 $\pm$ 229	-114 $\pm$ 232	-145 $\pm$ 252	-272 $\pm$ 196	-811 $\pm$ 193
GAIL	4059 $\pm$ 728	3722 $\pm$ 650	2960 $\pm$ 420	1134 $\pm$ 270	-413 $\pm$ 226
GAIL-Reward Only	-284 $\pm$ 77	-269 $\pm$ 111	-293 $\pm$ 106	-399 $\pm$ 97	-833 $\pm$ 77
GAIL-Expert-Noise	3481 $\pm$ 635	3314 $\pm$ 500	2806 $\pm$ 405	<b>1190</b> $\pm$ 262	<b>-411</b> $\pm$ 193
IMPLANT (ours)	<b>5240</b> $\pm$ 924	<b>4317</b> $\pm$ 486	<b>3259</b> $\pm$ 382	1182 $\pm$ 237	-416 $\pm$ 217

(b) HalfCheetah with transition noise

Sigma	0.0	0.001	0.002	0.005	0.01
BC	-359 $\pm$ 247	-368 $\pm$ 244	-360 $\pm$ 271	-402 $\pm$ 214	-426 $\pm$ 208
BC-Dropout	-99 $\pm$ 229	-138 $\pm$ 209	-115 $\pm$ 220	-128 $\pm$ 219	-139 $\pm$ 192
GAIL	4059 $\pm$ 728	4113 $\pm$ 600	4066 $\pm$ 748	3865 $\pm$ 687	3506 $\pm$ 640
GAIL-Reward Only	-284 $\pm$ 77	-271 $\pm$ 107	-266 $\pm$ 109	-287 $\pm$ 107	-293 $\pm$ 117
GAIL-Expert-Noise	3481 $\pm$ 635	3527 $\pm$ 527	3429 $\pm$ 616	3330 $\pm$ 633	3064 $\pm$ 683
IMPLANT (ours)	<b>5240</b> $\pm$ 924	<b>5212</b> $\pm$ 544	<b>5080</b> $\pm$ 486	<b>4716</b> $\pm$ 498	<b>4087</b> $\pm$ 444

TABLE IX: Raw results of Figure 2 in Walker2d environment

(a) Walker2d with motor noise

Sigma	0.0	0.1	0.2	0.5	1.0
BC	153 ± 162	152 ± 163	144 ± 161	55 ± 76	10 ± 13
BC-Dropout	344 ± 72	350 ± 80	345 ± 133	211 ± 139	25 ± 37
GAIL	3847 ± 635	3603 ± 830	2626 ± 1214	<b>608</b> ± 300	185 ± 155
GAIL-Reward Only	2 ± 5	32 ± 94	25 ± 78	12 ± 33	3 ± 9
GAIL-Expert-Noise	3437 ± 787	3456 ± 822	2570 ± 1285	572 ± 328	171 ± 166
IMPLANT (ours)	<b>4403</b> ± 242	<b>3666</b> ± 991	<b>2816</b> ± 1019	596 ± 336	<b>214</b> ± 148

(b) Walker2d with transition noise

Sigma	0.0	0.001	0.002	0.005	0.01
BC	153 ± 162	162 ± 171	156 ± 167	145 ± 166	119 ± 153
BC-Dropout	344 ± 72	338 ± 102	327 ± 124	302 ± 175	261 ± 168
GAIL	3847 ± 635	3835 ± 671	3689 ± 921	2096 ± 1412	856 ± 938
GAIL-Reward Only	2 ± 5	18 ± 67	22 ± 79	41 ± 95	18 ± 67
GAIL-Expert-Noise	3437 ± 787	3422 ± 779	3317 ± 879	2387 ± 1272	1147 ± 876
IMPLANT (ours)	<b>4403</b> ± 242	<b>4373</b> ± 307	<b>4202</b> ± 671	<b>2653</b> ± 1337	<b>1293</b> ± 1098

TABLE X: Imitation via PWIL on Hopper with motor noise

Sigma	0.0	0.1	0.2	0.5	1.0
PWIL	3552 ± 200	2189 ± 1236	935 ± 706	<b>393</b> ± 119	218 ± 86
IMPLANT w/ PWIL (ours)	<b>3563</b> ± 87	<b>2637</b> ± 1140	<b>1110</b> ± 817	390 ± 103	<b>232</b> ± 82

TABLE XI: Imitation via PWIL on Hopper with transition noise

Sigma	0.0	0.001	0.002	0.005	0.01
PWIL	3552 ± 200	3011 ± 958	1961 ± 1144	807 ± 500	<b>469</b> ± 319
IMPLANT w/ PWIL (ours)	<b>3563</b> ± 87	<b>3226</b> ± 739	<b>1982</b> ± 1079	<b>942</b> ± 649	452 ± 293